Noise Spectrum of Electron Beam in Longitudal Magnetic Field

Part II — The UHF Noise Spectrum

By W. W. Rigrod

(Manuscript received January 21, 1957)

Sharp peaks are found in the UHF spectrum (10 *to* 500 *mc*) *of an electron beam, emanating from a shielded diode. In the presence of a longitudinal magnetic field, the strongly rippled beam displays an additional set of peaks whose frequencies are proportional to the field strength. The largest of these, just above the cyclotron frequency, is connected with the overlap of a dense cluster of particle orbits, passing close to the beam axis. It can attain amplitudes of 65 db above background noise.*

The transverse distribution of UHF noise power is found to agree with that for ideal Brillouin flow, even in rippled beams. With long ripple wavelengths, two noise maxima are found to flank each beam waist. A small-signal wave analysis explains this pattern, and affords some insight into the energy-exchange processes in rippled-beam amplification. The reduction in "growing noise" due to positive ions is attributed to increased cancellation of net radial beam motion, due to overlap in particle orbits near the axis.

I INTRODUCTION

The reader is referred to Part I[1] for a description of the experimental apparatus and its operation. In this paper, measurements of noise power in the same electron beam are described, with frequencies chiefly in the 10- to 500-mc range, and relatively weak magnetic fields. For the UHF measurements, a calibrated coaxial step attenuator and a super-regenerative receiver (the Hewlett-Packard 417-A VHF Detector) are used. Relative noise-power amplitudes at fixed frequencies are measured as before, in terms of changes in attenuation between probe and receiver required to restore constant receiver output. To obtain qualitative information, however, such as the location of noise maxima along the beam, the series attenuation is fixed. The receiver output is amplified, rectified, and per-

mitted to register itself directly on the chart recorder, whose motion is synchronized with that of the probe. Very roughly, the detector output varies as the log of input power.

Measurements are described (a) of the UHF noise spectrum in the beam, just outside the gun anode; (b) of this spectrum at the end of the drift region, in a longitudinal magnetic field; (c) of the noise-power distribution along the axis; and (d) transverse to the axis of the rippled beam in the drift region. Two calculations are then outlined, one of wave propagation along the rippled beam (to explain the observed distribution patterns), and the other to account for some spectacular peaks in the beam spectrum (b).

II FIELD-INDEPENDENT PEAKS

When the noise spectrum of an electron beam is scanned by a tunable receiver, it is found that an irregular array of narrow-band peaks characterize the UHF region, below about 1000 mc. Of these peaks, some are due to spurious modulation effects,[2] and can be eliminated as follows:

(1) Transit-time oscillations due to positive ions, secondary electrons, or both. Such frequencies vary with probe (collector) position.

(2) Resonances in the probe and receiver, excited by the pulsed-voltage supply. These are unaffected by changes in collector current.

(3) Ion oscillations in the electron gun or beam. Their frequencies vary with anode voltage.

The remaining narrow-band peaks fall into two classes, depending on whether their frequencies vary with the magnetic field.

Well-defined peaks can be detected with the RF probe stationed one inch from the gun anode, with or without any focusing field. When the beam is focused by a longitudinal magnetic field, these disturbances propagate along the beam, and tend to increase in amplitude with distance, but not to change in frequency. A typical set of such frequencies, within the range of the tunable receiver is as follows: 15.9, 24.3, 31.2, 34.0, 48.5, 63.4, 77.0, 108, 151, 166, 270.5, 372 and 481 mc. (During this measurement, the anode voltage was 2,200, and the peak current about 40 ma.)

No consistent relation could be found between these frequencies and either the anode voltage or the cathode temperature, although unmistakable frequency changes did occur when these parameters were manipulated. Failure to establish such a relation may have been due to uncontrolled drift in cathode activity. In any case, the measurements did serve to narrow the field of possible mechanisms, by eliminating the following:

(1) Transverse positive-ion oscillations,[3] for which the frequencies vary as the square root of anode voltage.

(2) Transverse electron plasma oscillations (near or beyond the anode), for which the frequencies would be too high.

(3) Longitudinal electron plasma oscillations at the potential minimum, for the same reason (should be near 2,500 mc).

(4) Longitudinal diode oscillations.[4] When the electron transit angle through the diode is approximately $(n + \frac{1}{4})$ periods, where n is an integer, the real part of the diode conductance becomes negative, permitting oscillations to occur. Again the frequencies of such oscillations would be too high, (2,200 mc and higher) for the gun used, to conform to the observed values.

There is, however, one published theory for which an order-of-magnitude correspondence does exist between the measured and calculated frequencies. Klemperer[5, 6] has shown that a strip beam tends to break up into clusters of "pencils" at the cathode. He ascribes these to standing waves resulting from transverse oscillations in the space-charge cloud, and offers an expression for the wave velocity in this medium. Application of his formula to the cathode used in the present experiments results in a least frequency of 31.3 mc. Other observers, such as Smyth[7] and Veith,[8] have also reported evidence of interaction between electrons in a retarding-field region and RF fields, which may underlie these oscillations.

III FIELD-DEPENDENT PEAKS

With the RF probe stationed ten or more inches from the gun anode, narrow-band peaks can be found in the noise spectrum of the beam. The amplitudes of these peaks increase and their frequencies decrease with decreases in the magnetic field. For each probe position, the process of finding the peak of greatest amplitude involves repeated adjustments of the focusing field, the magnetic field at the cathode, and the receiver frequency.

When the fields have been so optimized, it is found that the probe is located at or near the first beam-diameter minimum, following that at the entrance to the drift space. When the field is doubled, and the "tuning" process repeated, the greatest peak is found to have about twice the frequency of the first, and the probe is found to be located at or near the second beam waist. It is convenient, therefore, to think of these peaks as "proper" frequencies of the $N = 1$, etc., modes of the rippled beam, where N is the number of ripple wavelengths between gun and probe.

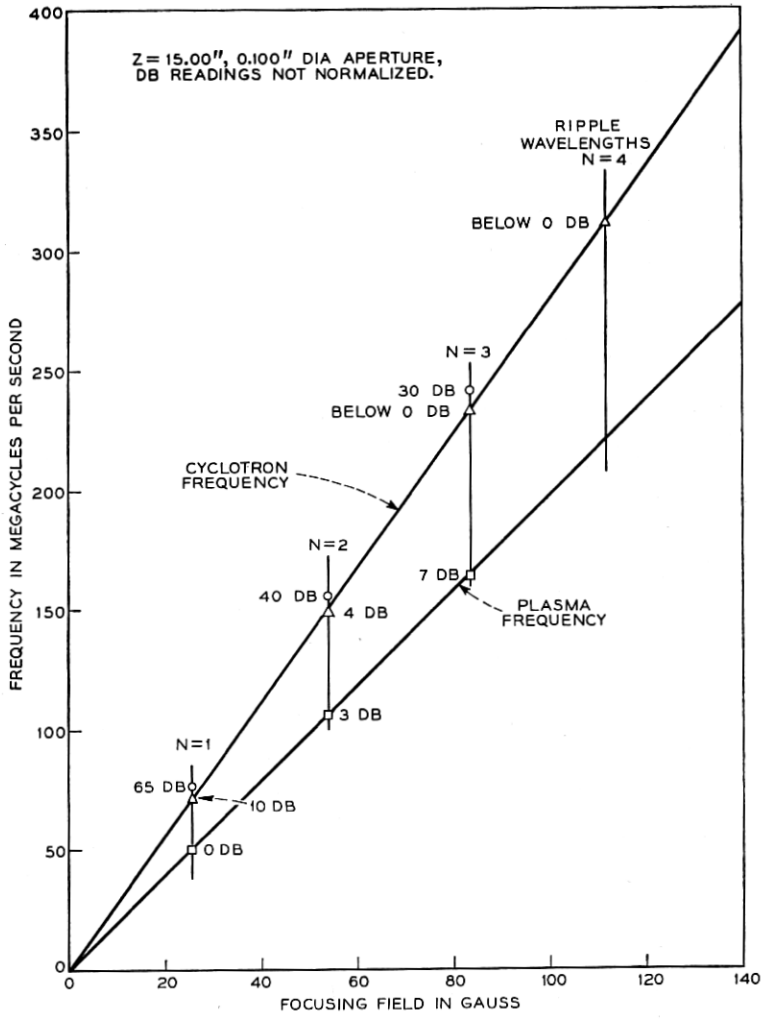

FIG. 1 — Frequencies and amplitudes of several narrow-band UHF peaks measured at a fixed probe position, about 16 inches from the gun anode. N is the number of beam-ripple wave-lengths between anode and probe. Other peaks have been observed at higher harmonics of the "proper" frequency (encircled points), and at about half that frequency.

As shown by the encircled points in Fig. 1, these frequencies range between 1.03 and 1.06 times the calculated cyclotron frequency, and have amplitudes as high as 65 db above the background noise. The amplitudes decrease with increasing N, falling off as the minus two-thirds power of the frequency.

At each of these optimum field settings, several weaker "satellite" peaks can also be detected, most readily those at the cyclotron frequency itself, and at 0.707 times the latter; i.e., the "plasma" frequency, as shown in Fig. 1. In addition, smaller peaks have been repeatedly observed at harmonics (up to the sixth) of the proper frequency, and one at slightly less than half of that frequency. (When a proper frequency was simulated by means of a signal generator, only its first harmonic could be detected in the receiver output.)

At the fields corresponding to $N = 4$ in Fig. 1, the cyclotron frequency (312 mc) was found, but not the proper frequency. The highest proper frequency observed was 240.5 mc, in the $N = 3$ mode. The proper-frequency peaks decrease with increasing focusing field, whereas the field-independent peaks excited in the electron gun tend to increase, at the far end of the drift region.

IV SPATIAL DISTRIBUTION OF UHF NOISE CURRENTS

In Figs. 2 to 5 are shown synchronized chart records of collector current, one or more UHF narrow-band peaks, and microwave noise power near 4,000 mc — all as functions of distance from the electron gun, for the $N = 1$ to 4 modes, respectively. In all runs, the beam was pulsed with a 1,000-cycle square wave, and the collector aperture set at a 0.100 inch diameter. The magnetic fields at the cathode and in the drift space were adjusted before each set of readings, with the probe at a common reference position, for greatest amplitude of some UHF peak. In Figs. 2 and 3, these were proper frequencies, whereas in Figs. 4 and 5 they were field-independent frequencies.

The content of these distribution curves can be summarized as follows:

(1) At the low fields employed (none quite equal to the nominal Brillouin value), the beam ripples are quite large, both in amplitude and wavelength.

(2) The proper-frequency traces have two or three maxima near each beam waist, and their amplitudes grow more rapidly with distance from the gun than any of the satellite frequencies.

(3) The patterns of the cyclotron and "plasma" frequencies do not differ significantly from those of the field-independent frequencies, and usually display two peaks near each beam waist.

(4) The collector-current maxima decrease with distance from the gun, although their minima change little. (The first maximum is sometimes flat-topped due to beam interception before it enters the drift space.) The rate of decrease of these maxima, and the rate of increase of proper-frequency amplitude, are greater, the longer the ripple wavelength.

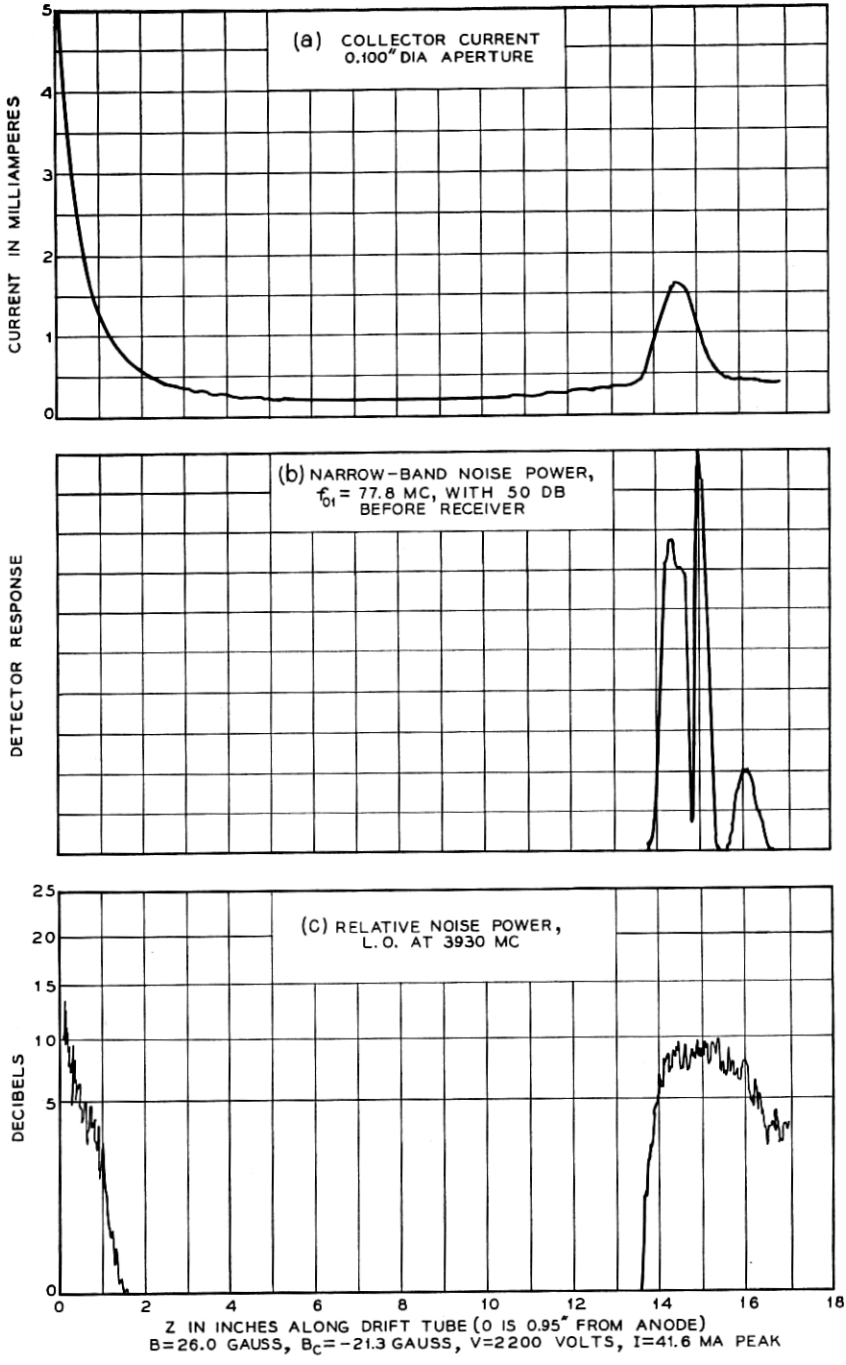

FIG. 2 — The fields have been adjusted for maximum amplitude of the $N = 1$ proper frequency, 77.8 mc, at a reference probe position ($z = 15$ inches). The synchronized probe records indicate three distinct maxima of this proper frequency near the beam waist.

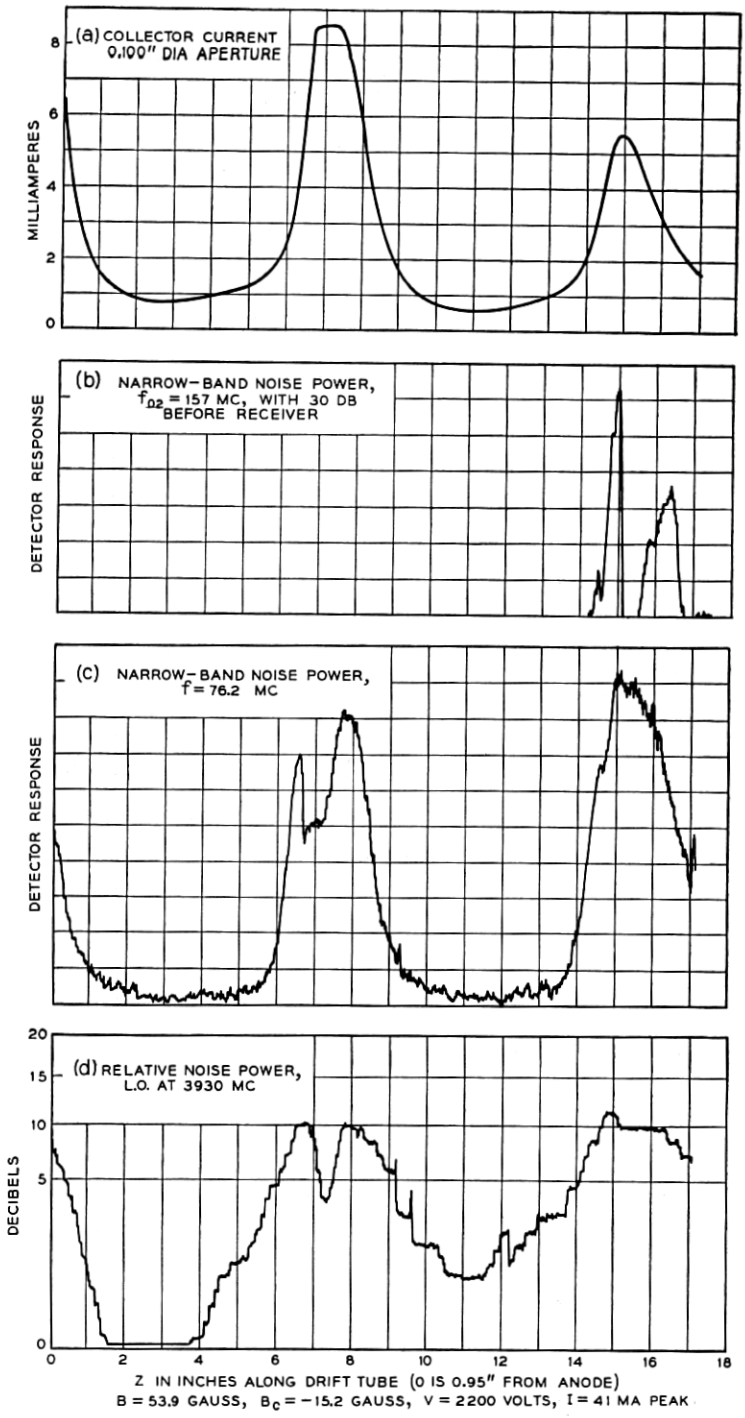

FIG. 3 — The longitudinal distributions of the $N = 2$ proper frequency, 157 mc, as well as its "satellite" 76.2 mc, and microwave noise power, are shown here, with fields adjusted for greatest amplitude of the proper frequency at $z = 15$ inches.

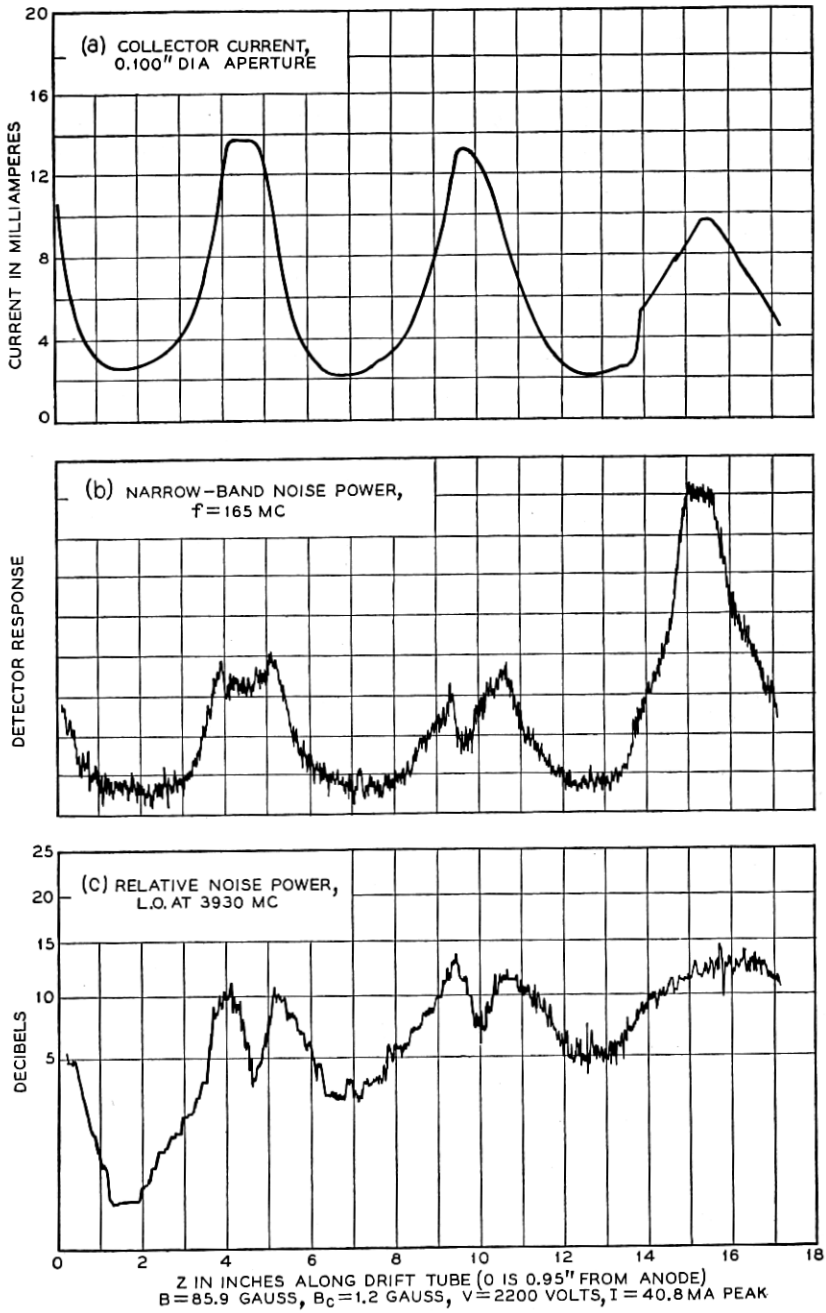

FIG. 4 — The fields have been adjusted for maximum amplitude, at the same reference probe position, of a wave excited in the diode, with frequency unaffected by the magnetic field, 165 mc. The cyclotron frequency for this field is 240.2 mc.

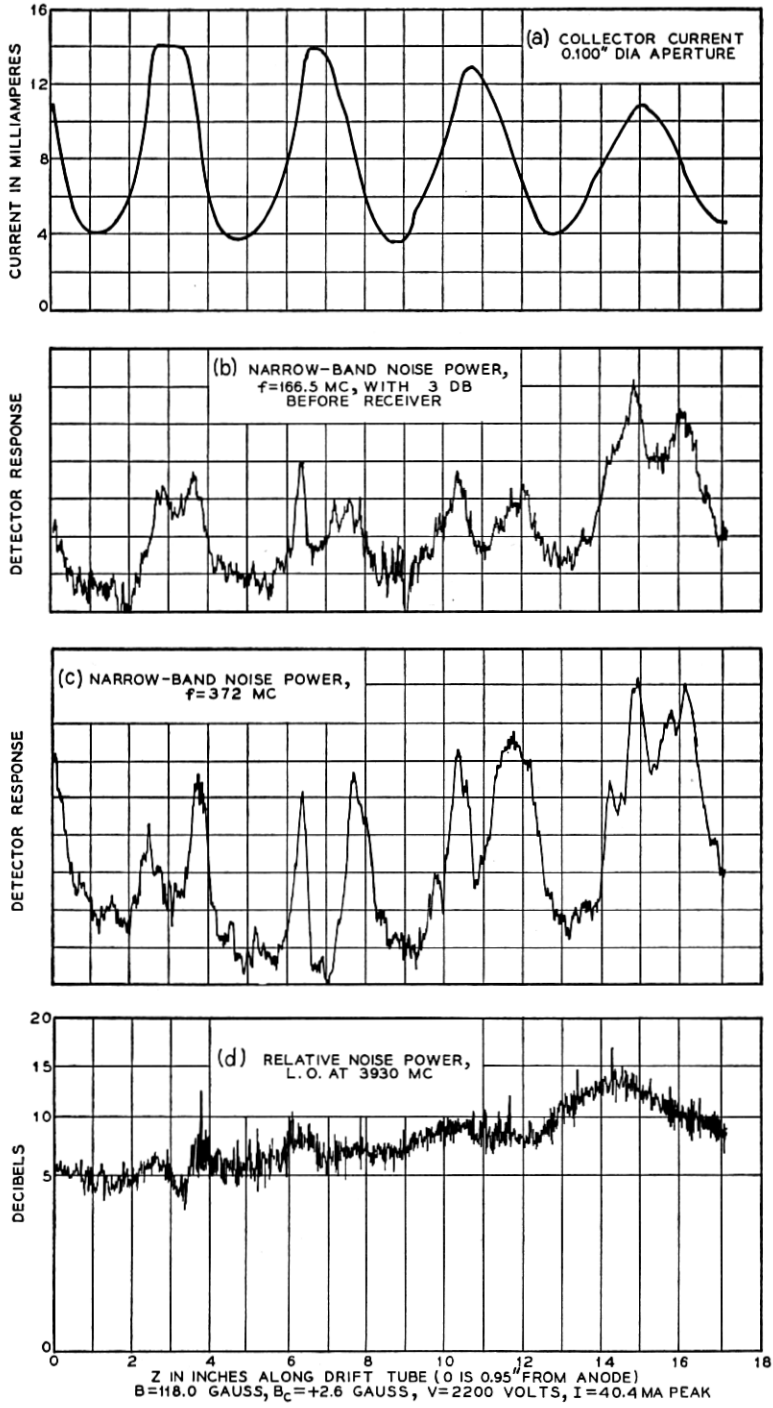

FIG. 5 — A procedure similar to that in Fig. 4 was followed, with four ripple wavelengths between anode and reference plane. The cyclotron frequency here is 329.5 mc.

(5) The patterns of microwave noise power resemble blurred envelopes of the UHF traces.

Some idea of the transverse distributions of UHF noise power and electron-current density, in a region of strong proper-frequency excitation, is given in Figs. 6 and 7. The measurements were taken by moving a small aperture in a broad arc through the probe centerline, just in front of the probe aperture. In both illustrations, the relative noise power has been "normalized" to compensate for variations in electron current traversing the RF gap.

The curves of Fig. 6 are typical of most such measurements. The beam-current density varies smoothly through a single broad maximum, and

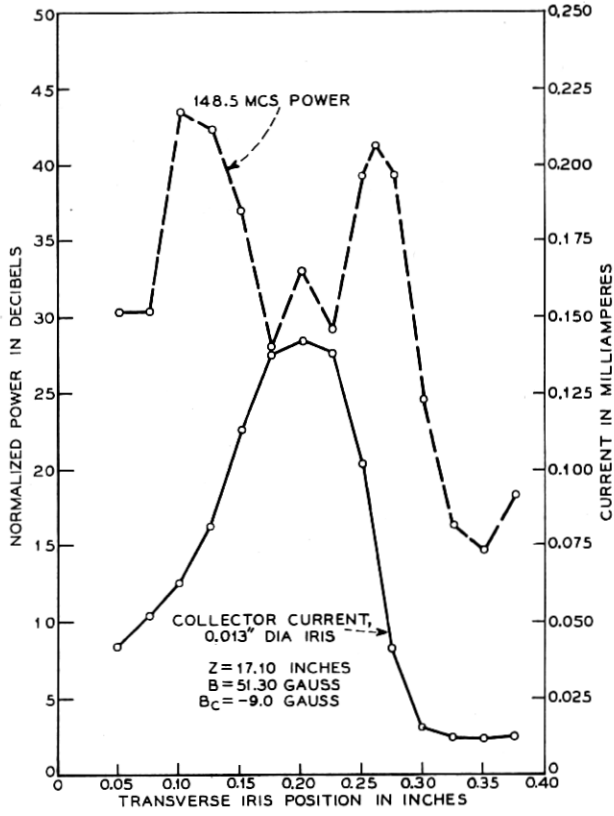

FIG. 6 — Simultaneous point-by-point measurements of collector current and relative noise power, obtained by moving an 0.013-inch diameter aperture in a broad arc through the probe centerline. The probe is stationary, about 18 inches from the gun anode, and the fields have been adjusted for maximum amplitude of the proper frequency, 148.5 mc. The cyclotron frequency is 143.8 mc.

the noise-power density is greatest at the rim of the beam so defined, and least near its center. No evidence of azimuthal periodicity was found. The curves of Fig. 7, which are less typical, indicate five distinct peaks of RF power, despite a nearly symmetrical pattern of collector current. At the time of this measurement, cathode emission may have been uneven, due to coating damage by ion bombardment.

In the rippled beam on which these measurements were made, the ratio of flux encircled at the cathode, to that in the drift space, was very small for most electrons. One would, therefore, expect the transverse noise-power distribution in this beam to resemble that in a smooth Brillouin beam.[9] The noise power expected when a pinhole aperture is located at the beam center can be compared with that when the aper-

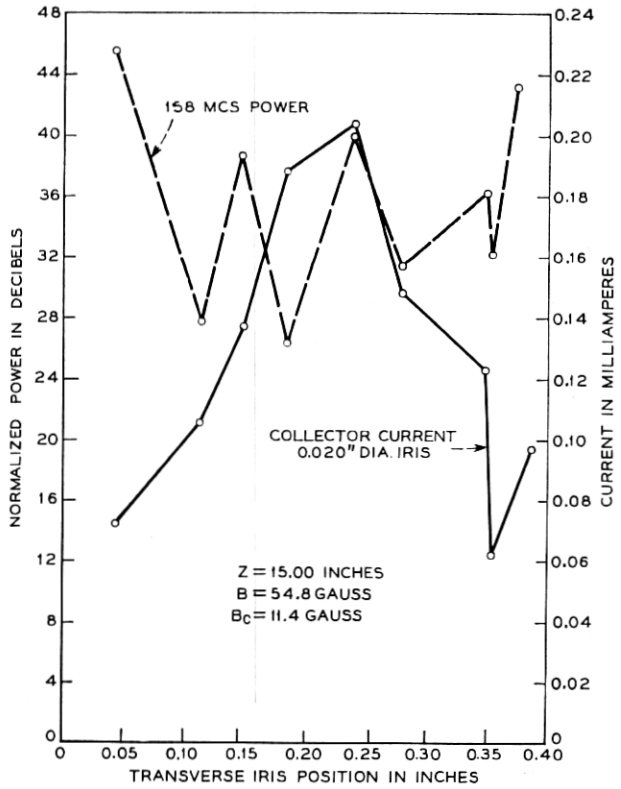

FIG. 7 — Transverse distribution measurements similar to those of Fig. 6. This pattern was obtained a week later than that of Fig. 6, and the cathode was operated at a higher temperature. The cyclotron frequency would be 153.2 mc for the field used.

ture straddles the beam rim, by taking the beam area exposed in the first case to be that of a sector of angle θ, and the length of beam surface in the second case to be that of the corresponding arc:

$$\frac{\text{Rf current sample inside of beam}}{\text{Rf current sample at rim of beam}} \cong \frac{\theta b^2 J_z}{2\theta b G_z} = \frac{b(\omega - \beta u)\cdot I_0(\beta b)}{2uI_1(\beta b)}.$$

Here b is the beam radius, and J_z, G_z the longitudinal components of volume and surface current densities, respectively. I_0 and I_1 are modified Bessel functions, β is the propagation constant, u the beam velocity, and ω the radian frequency. For the frequencies and beam radii employed in these measurements, this ratio is very much less than unity. Thus the pattern of Fig. 6 is in accord with this mode distribution. The multiple peaks of Fig. 7, however, do not conform to this picture, and are not understood at present.

As most of the RF power is concentrated near the rim of the beam, the question arises whether the double and triple peaks, in the longitudinal distribution patterns of Figs. 2 to 5, are not due to the probe aperture breaking through the beam rim. However, the dip between adjacent noise peaks is too great to be explained on the basis of reduced partition noise or weakened gap coupling, assuming the beam diameter there to be less than the gap diameter (0.100 inch). Moreover, double peaks occur even when the beam diameter exceeds the RF gap diameter; for instance, near the last three beam waists of Fig. 5. (When all of the beam is transmitted by the 0.100 inch aperture, the collector-current peak is flat-topped.) It seems likely, therefore, that the double and triple peaks correspond to peaks of amplitude over the entire beam cross-section.

V PROPAGATION ALONG THE RIPPLED BEAM

To find an explanation for the multiple peaks of space-charge current, a small-signal, slow-wave analysis of wave propagation along the rippled beam can be made, in which the special features of these experiments are exploited: long ripple wavelength, effectively no flux at the cathode, and low frequencies. The first of these features suggests that the propagation constants can be evaluated at each cross-section plane as though the beam were uniform, despite the presence of radial velocities. In addition, the space-charge density is assumed constant at each cross-section, and the electron flow laminar.

With these assumptions, the beam can be regarded as a fluid of moving charge, with a single-valued velocity at each point in space, as follows:

$$v_0 = (v_r , v_\theta , v_z) \tag{1}$$

where

$$v_r = r \cdot f(z), \qquad \text{or} \qquad \frac{\partial v_r}{\partial r} = \frac{v_r}{r}, \tag{2}$$

$$v_\theta = r\dot{\theta} = r\frac{\omega_c}{2}, \tag{3}$$

$$v_z = u. \tag{4}$$

Here, r, θ, z are the polar cylindrical coordinates, $\omega_c = \eta B$ the angular cyclotron frequency corresponding to the longitudinal focusing field B, and $f(z)$ a function describing the amplitude and spatial periodicity of the beam ripple. The experimental data indicates that the potential variations along the beam axis are negligible, permitting the assumption that the longitudinal velocity, u, is constant. MKS units are used.

Consistent with the distribution pattern of Fig. 6, the ac field can be represented by an axially-symmetric potential function, similar to that for the smooth Brillouin-flow beam:

$$V \sim I_0(\gamma r) \exp j(\omega t - \beta z), \tag{5}$$

$$\underline{E} = -\text{grad } V. \tag{6}$$

The ac equations of fluid motion are obtained by adding a small ac increment to each of the steady-state velocity components. In addition to the space-charge field, the ac electric field contributes forces acting on the charged medium; those contributed by the ac magnetic field are neglected:

$$\frac{d}{dt}(\underline{v}_0 + \underline{\tilde{v}}) = -\eta[-\text{grad } V - \text{grad } V_0 + (\underline{v}_0 + \underline{\tilde{v}}) \times \underline{B}]. \tag{7}$$

The ac velocity is distinguished by a tilde, and the dc velocity by a zero subscript. Here $\eta = e/m$ is the charge-mass ratio of the electron, a positive quantity. As all ac quantities are functions of spatial positions, their time differentiation (indicated by a dot) is equivalent to multiplication by $j(\omega - \beta u)$, written $j\omega_b$ for brevity.

The components of the force equation are expanded as follows:

$$\frac{\partial \tilde{v}_r}{\partial t} + (v_r + \tilde{v}_r)\frac{\partial}{\partial r}(v_r + \tilde{v}_r) + (u + \tilde{v}_z)\frac{\partial}{\partial z}(v_r + \tilde{v}_r) - \frac{(v_\theta + \tilde{v}_\theta)^2}{r} = \eta\frac{\partial V}{\partial r} + \eta\frac{\partial V_0}{\partial r} - \omega_c(v_\theta + \tilde{v}_\theta), \tag{8a}$$

$$\left[j\omega_b + v_r\left(\frac{\partial}{\partial r} + \frac{1}{r}\right)\right]\bar{v}_r + \left(\frac{\partial v_r}{\partial z}\right)\bar{v}_z = \eta\frac{\partial V}{\partial r}, \tag{8b}$$

$$\frac{\partial \bar{v}_\theta}{\partial t} + (v_r + \bar{v}_r)\left(\dot{\theta} + \frac{\partial \bar{v}_\theta}{\partial r}\right) + u\frac{\partial \bar{v}_\theta}{\partial z} + (v_r + \bar{v}_r)\left(\dot{\theta} + \frac{\bar{v}_\theta}{r}\right) = \eta\frac{\partial V}{\partial \theta} + \omega_c(v_r + \bar{v}_r), \tag{9a}$$

$$\left[j\omega_b + v_r\left(\frac{\partial}{\partial r} + \frac{1}{r}\right)\right]\bar{v}_\theta = 0, \tag{9b}$$

$$\frac{\partial \bar{v}_z}{\partial t} + v_r\frac{\partial \bar{v}_z}{\partial r} + u\frac{\partial \bar{v}_z}{\partial z} = \eta\frac{\partial V}{\partial z}, \tag{10a}$$

$$\left[j\omega_b + v_r\frac{\partial}{\partial r}\right]\bar{v}_z = -j\eta\beta V. \tag{10b}$$

An expression for the ac space-charge density, $\tilde{\rho}$, can be obtained in terms of its steady-state counterpart, ρ_0, by means of the charge-conservation equation:

$$\frac{\partial \tilde{\rho}}{\partial t} = -\underline{v}_0\cdot\text{grad}\ \tilde{\rho} - \underline{\bar{v}}\cdot\text{grad}\ \rho_0 - \rho_0\ \text{div}\ \underline{\bar{v}} - \tilde{\rho}\ \text{div}\ \underline{v}_0 - \underline{v}_0\cdot\text{grad}\ \rho_0 - \rho_0\ \text{div}\ \underline{v}_0\,. \tag{11}$$

As the beam diameter changes slowly, the dc space-charge density at each plane is taken to be inversely proportional to the square of the radius, b:

$$|\ \text{grad}\ \rho_0\ | = \frac{\partial \rho_0}{\partial z} = -\frac{2\rho_0}{b}\frac{\partial b}{\partial z} \cong -\frac{2v_r}{ur}\rho_0, \tag{12}$$

$$\text{div}\ \underline{v}_0 = -\frac{\underline{v}_0\cdot\text{grad}\ \rho_0}{\rho_0} \cong -\frac{2v_r}{r}, \tag{13}$$

$$\left[j\omega_b + v_r\left(\frac{\partial}{\partial r} + \frac{1}{r}\right)\right]\tilde{\rho} = -\rho_0\left[\frac{1}{r}\frac{\partial}{\partial r}(r\bar{v}_r) - j\beta\bar{v}_z\left(1 - j\frac{2}{\beta u}\frac{v_r}{r}\right)\right]. \tag{14}$$

At low frequencies (the UHF region),

$$\frac{\partial V}{\partial r} \ll \frac{V}{r}$$

as $(\gamma r)^2 \ll 1$. This inequality is also true of other ac quantities proportional to V, such as $\bar{v}_z$ and $\tilde{\rho}$, and with a small error can be assumed to be true for $\bar{v}_r$. When the operator $\partial/\partial r$ is omitted from (8), (9), (10), and (14), it is possible to solve explicitly for $\tilde{\rho}$ in terms of ρ_0 and V.

The laminar-flow rippled beam can be described by the particle trajectories, as follows:

$$r_i = r_{0i}(1 + \delta \cos \beta_c z), \tag{15}$$

where r_{0i} is the maximum radius for the particle considered, and $0 < \delta < 1$. For this model of the beam,

$$\frac{v_r}{r} = \frac{\dot{b}}{b} = \frac{-\delta\omega_c \sin \beta_c z}{1 + \delta \cos \beta_c z}, \tag{16}$$

$$\frac{1}{r}\frac{\partial v_r}{\partial z} = \frac{-\omega_c \beta_c \delta(\delta + \cos \beta_c z)}{(1 + \delta \cos \beta_c z)^2}. \tag{17}$$

The region of interest, judging from the observed peak locations, is not at the mid-plane of the beam waist, where $v_r = 0$, but on either side of that plane, where $| v_r/r |$ is greatest. It is readily found that, at these positions $(1/r)\ (\partial v_r/\partial z)$ is zero, and (14) can be written

$$\tilde{\rho} = \frac{\eta \rho_0 V}{\omega_b^2}\left[\frac{\gamma^2}{\left(1 - j\dfrac{v_r}{\omega_b r}\right)^2} - \beta^2 \frac{\left(1 - j\dfrac{2}{\beta u}\dfrac{v_r}{r}\right)}{\left(1 - j\dfrac{v_r}{\omega_b r}\right)}\right]. \tag{18}$$

This can be combined with Poisson's Equation,

$$\Delta V = (\gamma^2 - \beta^2)V = -\tilde{\rho}/\varepsilon, \tag{19}$$

to furnish a relation between γ and β:

$$\gamma^2\left[1 - \frac{R}{\left(1 - j\dfrac{v_r}{\omega_b r}\right)^2}\right] = \beta^2\left[1 - \frac{R\left(1 - j\dfrac{2}{\beta u}\dfrac{v_r}{r}\right)}{\left(1 - j\dfrac{v_r}{\omega_b r}\right)}\right] \tag{20}$$

where $R = \omega_p^2/\omega_b^2$ and $\omega_p^2 = -\eta\rho_0/\epsilon$, the square of the angular plasma frequency.

At the beam boundary, $r = b$, the continuity of the tangential field components and the change in radial electric displacement can be expressed in the form of an admittance equation:

$$\left[\frac{1}{V}\left(\frac{\partial V}{\partial r} - \frac{\tilde{\sigma}}{\epsilon}\right)\right]_b^{\mathrm{I}} = \left[\frac{1}{V}\frac{\partial V}{\partial r}\right]_b^{\mathrm{II}}. \tag{21}$$

Here I refers to the beam, $0 \leqq r \leqq b$, and II to the space between beam and the concentric conducting tube, $b \leqq r \leqq a$. The surface charge layer, $\tilde{\sigma}$, takes account of the surface ripple, of amplitude $\tilde{r}$:

$$\tilde{\sigma} = \rho_0 \tilde{r} = -\frac{j\rho_0 \tilde{v}_r}{\omega_b},$$

$$-\tilde{\sigma}/\epsilon = -\frac{R(\partial V/\partial r)}{1 - j\dfrac{v_r}{\omega_b r}}. \tag{22}$$

The appropriate potential functions in I and II are reduced by means of the low-frequency, or thin-beam, approximation, as follows:

$$\left[\frac{1}{V}\frac{\partial V}{\partial r}\right]_b^{\mathrm{I}} = \frac{\gamma I_1(\gamma b)}{I_0(\gamma b)} \cong \frac{\gamma^2 b}{2},$$

$$\left[\frac{1}{V}\frac{\partial V}{\partial r}\right]_b^{\mathrm{II}} = \beta\left[\frac{I_1(\beta b)K_0(\beta a) + I_0(\beta a)K_1(\beta b)}{I_0(\beta b)K_0(\beta a) - I_0(\beta a)K_0(\beta b)}\right] \tag{23}$$

$$\cong \frac{\beta^2 b}{2} - \frac{1}{b \ln a/b}$$

where the following small-argument approximations have been used:

$$K_0(x) \cong -\ln x,$$

$$K_1(x) \cong \frac{x}{2}\ln x + \frac{1}{x}. \tag{24}$$

The boundary equation thus provides a second relation between γ and β:

$$\frac{\gamma^2 b}{2}\left[1 - \frac{R}{\left(1 - j\dfrac{v_r}{\omega_b r}\right)}\right] = \frac{\beta^2 b}{2} - \frac{1}{b \ln \dfrac{a}{b}}. \tag{25}$$

For the smooth beam in Brillouin flow ($v_r = 0$), the boundary equation, to the same low-frequency approximation, is as follows:

$$R_0 \equiv \frac{\omega_p^2}{(\omega - \beta_0 u)^2} = \frac{2}{(\beta_0 b)^2 \ln \dfrac{a}{b}}. \tag{26}$$

To see how the beam ripple affects the propagation constant, it is sufficient to find its first-order effect; i.e., to assume relatively small radial velocities and find a solution for β which is not very different from its value, β_0, for the smooth beam:

$$\beta = \beta_0 + \delta = \beta_e \pm \beta_q + \delta, \tag{27}$$

where

$$|\delta| \ll \beta_0\,; \qquad \beta_q \cong \frac{\omega_p}{u\sqrt{R_0}}\,; \qquad \beta_e = \frac{\omega}{u}.$$

In addition, $| v_r/\omega_b r |$ is less than unity, and $| 2v_r/\beta ur |$ can be neglected entirely. With these assumptions, the boundary and characteristic equations can be combined to solve for β:

$$\frac{\gamma^2}{\beta^2} = \frac{F(F - R)}{F^2 - R} = \frac{F - \left(\frac{\beta_0}{\beta}\right)^2 R_0}{F - R}, \tag{28}$$

where

$$F = 1 - j\frac{v_r}{\omega_b r}.$$

Utilizing the low-frequency condition, $| R^2 | > | R | > 1$, this equation can be reduced and, after some algebra, solved:

$$\frac{\beta_0}{\beta}\left(\frac{R_0}{R}\right)^{1/2} = \frac{\beta_0(\delta \pm \beta_q)}{(\beta_0 + \delta)(\pm\beta_q)} \cong 1 - j\frac{v_r}{2\omega_b r},$$

$$\beta_s \cong \beta_e + \beta_q - j\frac{v_r}{2ur}, \tag{29a}$$

$$\beta_f \cong \beta_e - \beta_q + j\frac{v_r}{2ur}. \tag{29b}$$

These expressions show that the current in the slow wave (I_s) will grow when (v_r/r) is negative; i.e., when the beam is contracting, and decrease during its expansion. The fast wave (I_f) will do the opposite. In probe measurements along the beam, the detected ac power is proportional to the square of the total space-charge current, which has the following dependence on time and distance when the amplitudes of both waves are initially equal:

$$(I_s + I_f) = 2I_{\max} \cos(\omega t - \beta_e z) \cdot \cos(\beta_q z) \cdot \sinh\left(\frac{V_r z}{2ur}\right). \tag{30}$$

In UHF noise-power measurements along beams with long ripple wavelengths, the two planes of maximum $\pm (v_r/r)$ are separated by only a small fraction of a space-charge wavelength. Therefore, $\cos \beta_q z$ at the first of these planes is only slightly larger than at the second. Thus, two peaks of current are observed, in agreement with (30). By contrast, in rippled-beam amplification at microwave frequencies, shorter ripple wavelengths and smaller ripple amplitudes are employed. Then (v_r/r) varies nearly sinusoidally over the ripple wavelength. For maximum net gain per ripple, maximum negative (v_r/r) is adjusted to coincide with the plane of $\cos \beta_q z = 1$ (maximum current), and maximum positive (v_r/r) at the current minimum, half a wavelength beyond.

The gain constants in (29) are independent of frequency. The net gain per ripple wavelength, however, will vary with frequency, depending on how closely both the current maxima and minima coincide with the regions of maximum $\pm (v_r/r)$, respectively. This is a statement of the "resonance" condition between ripple wavelength and half the space-charge wavelength, which emerges from one-dimensional analyses[10] of this gain mechanism based on transmission-line analogies.

Such analyses generally assume small-amplitude sinusoidal variations of the reduced plasma wave number, β_q, along a one-dimensional beam in a longitudinal ac field with no losses. Periodic variations in either beam or wall diameters, or beam velocity, cause the beam "impedance" to vary periodically, imparting to it narrow-band filter-like properties equivalent to narrow-band signal gain. From another point of view,[11] these periodic impedance changes couple the fast and slow space-charge waves to each other intermittently, thereby effecting an energy transfer from the fast to the slow wave. As this coupling is lossless, I_s increases and I_f decreases with drift distance, in such a way as to keep their product constant. Then the product $I_{\max}I_{\min}$ increases, and the ratio $I_{\max}/_{\min}$ correspondingly decreases. In the case of *noise-power* amplification, two uncorrelated space-charge standing waves are present. Because the two slow waves cannot simultaneously be amplified at the expense of the two fast waves, the product $I_{\max}I_{\min}$ must remain constant.

The observed noise-current patterns in rippled-beam amplification,[1] however, are characterized by a *nearly constant ratio* $I_{\max}/I_{\min}$, and an *increase in the product* $I_{\max}I_{\min}$ along the beam, despite the fact that the beam voltage is fixed. This apparent contradiction can be resolved by a closer look at the energy-exchange processes.

Chu[12] has shown that the kinetic power flow in space-charge waves (the major part of the total power) is equal to the difference in powers carried by the fast and slow waves. This is equally true of beams with transverse motions and fields.[13] In rippled-beam amplification, whether analyzed as a modulated linear beam or at each beam cross-section separately, as here, the propagation constants are found to be complex conjugate quantities, whose real parts describe the ordinary fast and slow waves of a uniform beam. From either point of view, therefore, a decrease in I_f and an increase in I_s signifies an increase in the negative kinetic power flow carried by the waves, or a decrease in the total kinetic energy of the beam.

As shown in (29), the gain constants are proportional to v_r, indicating that the dc energy transferred to the waves when the beam contracts could only have come from the *radial* kinetic energy, not the longitudinal.

The direction of energy transfer is reversed during the subsequent beam expansion. If the ripple were perfectly symmetrical, therefore, and the dc-ac energy exchange perfectly reversible, the net effect of a beam ripple would be zero. Neither of these conditions is quite true in actual beams. Rippled flow is never truly laminar, and $|v_r/r|$ usually decreases with drift distance as the flow loses coherence; i.e., it is greater in beam contraction than in the next expansion. This by itself would produce a net gain per ripple in I_s, and a net loss in I_f, of equal amounts. In addition, however, unavoidable small non-linearities in electron motions prevent all of the ac energy in a de-amplified wave from being converted back to dc kinetic energy. Thus it is possible for *both* the fast and slow waves to increase in a ripple wavelength, the latter always more than the former.

The greater gain of the slow wave entails a loss of radial kinetic energy, in agreement with the observation that the ripple amplitude always decays more rapidly when rippled-beam amplification takes place. The incomplete reversibility of the ac-dc energy exchange probably accounts for the observed increase in $I_{max}I_{min}$ for noise currents. Finally, the net amplification of all of the space-charge waves, fast as well as slow, is in accord with the observed near-constancy of the ratio I_{max}/I_{min} for microwave-frequency noise, despite increases in the product $I_{max}I_{min}$ of 30 db and more.

VI ORIGIN OF THE PROPER-FREQUENCY PEAKS

Of the various peaks in the beam's noise spectrum, described in Section III and Fig. 1, those with "proper frequencies," slightly above the cyclotron value, are so large in amplitude that even an approximate analysis should be able to account for them. To do so, a "working model" of the beam is needed, which conforms to the experimental conditions which existed during the observations:

(1) The peak intensities were greatest near the middle of each beam waist, and decreased with decrease in ripple amplitude.

(2) The focusing field was below the nominal Brillouin value. The field at the cathode, B_c, was finite and opposed to the main field, B.

(3) Collector-current measurements along the beam axis showed the ratio of maximum to minimum current to be greater, the smaller the aperture.

(4) The gas pressure was about 10^{-7} mm Hg. The beam was pulsed with a 1,000-cycle square wave.

Item (3) indicates that the flow was non-laminar; and Item (4) indicates the presence of positive ions. All the items are consistent with the following picture:

In a beam with large ripples, nearly all electrons have their maximum radii and zero radial velocity at the same z-plane. Those with sufficiently large maximum radius will have enough transverse kinetic energy to surmount the space-charge forces at the beam waist, and pass through or close to the axis. Others, with smaller maximum radii, will spiral about that axis. Dolder and Klemperer[14] have observed a similar division of electrons into "crossovers" and non-crossovers, in electron-optical systems without magnetic fields.

Positive ions tend to neutralize the electronic space charge at the beam waists, broadening the region in which crossover occurs. The crossover trajectories thereupon overlap one another, resulting in multivalued transverse particle velocities in this region. In a first-order (linearized) study of wave propagation along the beam, one must replace the actual multivelocity charge motions with a single "fluid" of charge, whose velocity at any point is the average of the particle velocities there. It is clear that the z-velocity of the stream is u, and the radial velocity zero. The tangential velocity, $v_\theta = (\dot{\theta}r)_{\text{av}}$, however, is more complicated.

Owing to the partial or total neutralization of electronic space charge at the beam waists, and their large radii elsewhere, the crossover electrons will encounter virtually no space-charge forces in their paths. Their transverse paths will consequently be circles about fixed centers, described with angular velocity equal to the cyclotron frequency. Their angular velocity about the beam axis is given by Busch's Theorem:

$$\dot{\theta} = \frac{\omega_c}{2}\left[1 + \frac{K}{r^2}\right],$$

where

$$K = -r_c^2\left(\frac{B_c}{B}\right) = r_{\max} r_{\min} \tag{31}$$

is a positive quantity, as B_c/B is negative. Here, r_c is the radius at which a particular electron left the cathode, and r is its radius in the drift region. The angular velocity, $\dot{\theta}$, is greater than $\omega_c/2$ at all times, and exceeds ω_c in the waist region of the beam. The average value of v_θ at any point here, therefore, is greater than $\omega_c r$ and presumably varies from point to point in some unknown way.

If v_θ is left unspecified, and the assumptions adopted of zero space-charge forces and radial velocity over a finite length of beam:

$$\eta\frac{\partial V_0}{\partial r} = 0, \qquad v_r = 0, \qquad \frac{dv_r}{dt} = 0, \tag{32}$$

the radial component of the force equation (7) in Euler coordinates can

be written as follows:

$$\left(\frac{dv_0}{dt}\right)_r = -\frac{v_\theta^2}{r} = -\omega_c v_\theta , \tag{33}$$

$$v_\theta = 0 \quad \text{and} \quad \omega_c r. \tag{34}$$

Thus, the radial "balance" conditions (32) are consistent with either of two values for v_θ, of the equivalent stream with single-valued velocities. As it develops that either of these values leads to the same result, the first one will be used here for simplicity, $v_\theta = 0$.

An ac traveling wave along this beam cannot have any θ-dependency, because the beam has no single value of angular velocity $\dot{\theta}$, which might remain in synchronism with that of the wave. Thus, the perturbed dynamics equation (7) can be expanded, with the assumptions of an axial-symmetric ac field given by (5) and (6), a stream with steady-state velocity (0, 0, u), constant space-charge density ρ_0, and no space-charge forces, as follows:

$$\frac{\partial \tilde{v}_r}{\partial t} + u\frac{\partial \tilde{}_r}{\partial z} = \eta\frac{\partial V}{\partial r} - \omega_c \tilde{v}_\theta ,$$

$$\frac{\partial \tilde{v}_\theta}{\partial t} + u\frac{\partial \tilde{}_\theta}{\partial z} = \omega_c \tilde{v}_r ,$$

$$\frac{\partial \tilde{v}_z}{\partial t} + u\frac{\partial \tilde{v}_z}{\partial z} = \eta\frac{\partial V}{\partial z}.$$

These are solved for the ac velocity components:

$$\tilde{v}_r = \frac{-j\eta\omega_b}{\omega_b^2 - \omega_c^2}\frac{\partial V}{\partial r}, \tag{35}$$

$$\tilde{v}_\theta = -\frac{j\omega_c}{\omega_b}\tilde{v}_r , \tag{36}$$

$$v_z = -\frac{\eta\beta}{\omega_b} V. \tag{37}$$

With grad ρ_0 = div $\underline{v}_0 = 0$, the charge-conservation equation (11) can be solved for $\tilde{\rho}$:

$$\frac{\partial \tilde{\rho}}{\partial t} = -\underline{v}_0 \cdot \text{grad}\ \tilde{\rho} - \rho_0 \operatorname{div} \underline{\tilde{v}},$$

$$\tilde{\rho} = \frac{j\rho_0}{\omega_b}\operatorname{div}\underline{\tilde{v}} = \eta\rho_0\left[\frac{\gamma^2}{\omega_b^2 - \omega_c^2} - \frac{\beta^2}{\omega_b^2}\right]. \tag{38}$$

At very large ripple amplitudes, it is a fair assumption that the density of non-crossover electrons is negligible relative to that of crossovers in this region. Poisson's equation (19) can then be combined with the

above expression to obtain the characteristic equation:

$$\left(\frac{\beta}{\gamma}\right)^2 = \frac{1 - \dfrac{\omega_p^2}{\omega_b^2 - \omega_c^2}}{1 - \dfrac{\omega_p^2}{\omega_b^2}}. \tag{39}$$

In a frame of reference moving with the stream, u' is 0, $\beta' u'$ is 0, and $\omega_b' = \omega$. Then,

$$\left(\frac{\beta'}{\gamma'}\right)^2 = \frac{(\omega^2 - \omega_c^2 - \omega_p^2)\omega^2}{(\omega^2 - \omega_p^2)(\omega^2 - \omega_c^2)} \tag{40}$$

and β' becomes an infinite imaginary quantity when ω is ω_c. The phase velocity in the moving frame is infinite, as the real part of β' is zero; therefore the phase velocity v_p in the rest frame is also infinite. Thus, there is no Doppler shift in the "resonant" frequency observed in the rest frame:

$$\omega_{\text{observed}} = \frac{\omega_c}{1 - \dfrac{u}{v_p}} = \omega_c. \tag{41}$$

As the actual beam has a z-velocity spread, the field is never perfectly uniform, and as the calculation is valid for small ac quantities only, the discrepancy between this result and the observed "proper" frequencies, which were 1.03 to 1.06 times the cyclotron value, is not unexpected.

The singularity in (40) is seen to disappear when $\omega_p^2 = 0$. This indicates that an exact calculation would show the gain constant $(-j\beta)$ to increase with ρ_0, the density of the crossover electrons. Their trajectories, described by (31), and the absence of space-charge forces are such that $K = r_{\max} r_{\min}$; that is, the greater $r_{\max}$, the smaller $r_{\min}$, the distance of closest approach to the axis. Thus, a larger ripple amplitude (permitted by a lower magnetic field) produces a greater electron density in the waist region, and accordingly a greater oscillation amplitude at the resonant frequency, as observed.

The foregoing mathematics describes a form of resonance, the infinite phase velocity corresponding to longitudinal "cutoff" in a waveguide. Unlike a waveguide, however, the disturbance increases rather than attenuates along the axis, due to the transfer of dc kinetic energy (represented by v_θ^2/r) to the ac fields (excited by noise fluctuations at the cathode), at the cyclotron frequency ω_c.

Except for the direction of energy transfer, the situation is analogous to that of a low-pressure gas in a uniform magnetic field, when stressed by an impressed ac field of varying frequency. It has been found that the breakdown field at the cyclotron frequency is very much less than

at other frequencies.[15] Here the energy supplied by the ac field is coupled most effectively to the free electrons at the resonant frequency, increasing their dc kinetic energy until the gas breaks down. The circular ac charge motions due to the dc magnetic and the ac electric fields are superimposed on high-velocity random motions, similar to the radial motions in the drifting beam.

The UHF peaks observed at harmonics of the proper frequency may simply be due to the non-linear character of the beam, when excited by the high-level fundamental oscillations. The other faint satellite peaks, near 0.5 ω_c and 0.707 ω_c, seem to be associated with the unneutralized space-charge density at the beam waist.

The conspicuous role played by crossover electrons in the waist region of rippled beams, due to the tendency of their orbits to overlap there, leads one to re-examine their influence on rippled-beam amplification. As seen in the previous section, this gain process depends on the average value of (v_r/r) at each cross-section plane of the beam. The fraction of all electrons which penetrate to the beam axis depends on competition between the unneutralized space-charge forces and the particle's transverse kinetic energy. An increase in positive ion density tends to make the potential depressions at beam waists broader and shallower, and thereby increase the number of crossover electrons as well as the axial distance over which they reach the axis. The net effect is to reduce the average value of $| v_r |$ over a greater portion of the ripple wavelength, and thus reduce the net gain of the space-charge wave. This may explain why the "growing noise" phenomenon tends to be inhibited by an increase in positive ion density.

VII CONCLUSIONS

Evidence is found of oscillations with frequencies in the 10- to 500-mc region inside of an electron-gun diode. There is some basis for associating them with electron-field interaction in the retarding region of the diode. Another type of narrow-band noise peak is found near the waists of a strongly rippled beam in a longitudinal magnetic field, with frequencies proportional to the field strength. The strongest of these, at about 1.05 times the angular cyclotron frequency, ω_c, as well as its harmonics, can be explained by the resonant behavior of a short section of the beam, in which the average transverse velocity is nullified by overlap in particle orbits. Fainter satellite peaks, near 0.5 ω_c, 0.707 ω_c, and ω_c, respectively, accompany the dominant frequency.

In a drifting beam launched from a shielded electron gun and focused by an axial field, the transverse distribution of noise (or signal) intensity is found to agree with that predicted for ideal Brillouin flow. Despite

the presence of thermal motions and beam ripples, the ac power is found to be concentrated chiefly at the rim of the beam. Occasionally, several concentric rings of noise maxima are found within the beam, possibly due to unusual cathode conditions.

When the ripple wavelength is very long, two maxima of noise power are observed to flank each beam waist. A first-order calculation of wave propagation along a rippled laminar-flow beam accounts for this pattern by showing that space-charge waves grow at the expense of dc kinetic energy in the radial charge motion. In rippled-beam amplification of noise, the product $I_{max}I_{min}$ has been found to increase, and the the ratio I_{max}/I_{min} remain nearly constant, because both fast and slow waves are amplified, the former less than the latter, and because the wave coupling is not lossless.

Positive ions tend to collect at the waist of rippled beams, thereby extending the region in which electrons pass close to the axis, instead of circling about it. The overlap of their orbits leads to net cancellation of radial charge motion, and hence a reduction in rippled-beam amplification. This may explain why positive ions tend to inhibit the "growing noise" phenomenon.

REFERENCES

1. W. W. Rigrod, Noise Spectrum of Electron Beam in Longitudinal Magnetic Field. Part I — The Growing Noise Phenomenon, p. 831 of this issue.
2. C. C. Cutler, Spurious Modulation of Electron Beams, Proc. I.R.E., **44,** p. 61, Jan., 1956.
3. K. G. Hernquist, Plasma Ion Oscillations in Electron Beams, J. Appl. Phys. **26,** p. 544, May, 1955.
4. F. B. Llewellyn and A. E. Bowen, The Production of UHF Oscillations by Diodes, B.S.T.J., **18,** p. 280, April, 1939.
5. O. Klemperer, Influence of Space Charge on Thermionic Emission Velocities, Proc. Royal Soc. (London) (A) **190,** p. 376, 1947.
6. K. T. Dolder and O. Klemperer, High Frequency Oscillations in the Space Charge of some Electron Emission Systems, Journal of Electronics, **1,** p. 601 May, 1956.
7. C. N. Smyth, Total Emission Damping with Space-Charge-Limited Cathodes, Nature, **157,** p. 841, June 22, 1946.
8. W. Veith, Electron Energy Distribution in Space-Charge-Limited Electron Streams, Zeit. f. angew. Physik, **7,** No. 9, p. 437, 1955.
9. W. W. Rigrod and J. A. Lewis, Wave Propagation Along a Magnetically-Focused Cylindrical Electron Beam, B.S.T.J., **33,** p. 399, March, 1954.
10. R. W. Peter, S. Bloom, and J. A. Ruetz, Space-Charge-Wave Amplification Along an Electron Beam by Periodic Change of the Beam Impedance, RCA Rev., **15,** p. 113, March, 1954.
11. J. R. Pierce, The Wave Picture of Microwave Tubes, B.S.T.J., **33,** p. 1343, Nov., 1954.
12. L. J. Chu, 1951 I.R.E. Electron Tube Conference on Electron Devices.
13. H. A. Haus and D. L. Bobroff, Small Signal Power Theorem for Electron Beams (to be published).
14. K. T. Dolder and O. Klemperer, Space-Charge Effects in Electron Optical Systems, J. App. Phys., **26,** p. 1461, Dec., 1955.
15. S. J. Buchsbaum and E. Gordon, Highly Ionized Microwave Plasma, M.I.T. R.L.E. Quarterly Prog. Rep., p. 11, Oct. 15, 1956.